Desalination and Water Treatment
www.deswater.com
doi: 10.1080/19443994.2015.1020513

57 (2016) 8420–8436
April

Taylor & Francis
Taylor & Francis Group

Synthesis of oak gall tannin-immobilized hexagonal mesoporous silicate (OGT-HMS) as a new super adsorbent for the removal of anionic dye from aqueous solution

Ehsan Binaeian[a], Nasser Seghatoleslami[a,*], Mohammad Javad Chaichi[b]

[a]*Faculty of Engineering, Chemical Engineering Department, Ferdowsi University of Mashhad, Mashhad, Iran, Tel. +98 11 33209948; email: ehsan.binaeian@yahoo.com (E. Binaeian), Tel. +98 51 38805033; email: slami@um.ac.ir (N. Seghatoleslami)*
[b]*Faculty of Chemistry, University of Mazandaran, Babolsar, Iran, Tel. +98 11 35302386; email: jchaichi@yahoo.com*

Received 16 September 2014; Accepted 13 February 2015

ABSTRACT

Tannin as a natural biomass has been extracted from oak gall and was immobilized on hexagonal mesoporous silicate (HMS) in order to remove direct yellow 86 (DY86) from aqueous solution. The characteristics of the oak gall tannin-HMS adsorbent were substantiated by different techniques such as FTIR, TEM, TGA, BET, and XRD. From the BET analysis, a decline of 75.61% for the surface area of HMS nanoparticles was observed and indicates the proper coating through tannin. In order to analyze the adsorption data, five different isotherms were utilized and nonlinear regression scheme was employed using MATLAB software. It was concluded from the Langmuir isotherm that the maximum monolayer adsorption capacity was 435.5 mg g^{-1}. The thermodynamic analysis of this study also revealed that the adsorption was feasible, since the process was spontaneous and endothermic. The findings also indicate that the adsorption of DY86 follows the pseudo-second-order kinetic model.

Keywords: Oak gall tannin; Direct yellow 86; Adsorption; Hexagonal mesoporous silicate (HMS)

1. Introduction

Over the years, thousands tones of different types of dyes including harmful, toxic, and carcinogen materials are discharged to the aquatic environment. Dyes are used in various industries like dyestuffs textile, paper, plastics, and pharmaceuticals. With the growth of population and industry, the contamination of the environment and surface water became the real human beings' difficulty. Therefore, some dyes should be removed from waste waters due to their toxic natures. Direct yellow 86 (DY86) as an anionic dye has been employed in a range of industries such as silk, wool, leather, jute, cotton dying, biological staining, dermatology, veterinary medicine, green ink manufacture, textile dying, and paper printing [1]. DY86 is very poisonous and could harm human beings or animal's eye; therefore, it should be removed from the environment. Dye treatments are carried out either by physical or chemical treatments [2]. Chemical treatments for the removal of dye include coagulation or flocculation, electrical flotation, coagulation with Ca $(OH)_2$, electro coagulation, ionization, and electrochemical processes. On the other hand, some of the physical processes include membrane filtration,

*Corresponding author.

nanofiltration, reverse osmosis, electrodialysis, and adsorption. From the above processes, dye treatment for adsorption purposes is the most common method due to its feasibility features and high throughput [3]. Nowadays, natural materials are acknowledged as suitable source of low-cost adsorbents for removal of different pollutants and dyes from aqueous solutions.

Several natural adsorbents have been utilized by researchers for dye removal, namely waste sugar beet pulp [4], degreased coffee bean [5], garlic peel [6], pumpkin seed hull [7], beech wood sawdust [8], biomass fly ash [9], olive pomace [10], orange peel activated carbon [11], potato plant wastes [12], and cotton plant wastes [13].

Tannin is a natural growing plant that contains high content of multiple phenolic hydroxyls; thus, tannins can be used as an adsorbent for adsorption of some dyes and heavy metal ions. Tannin is water-soluble; therefore, it should be immobilized on water-insoluble supports such as agarose, cellulose, silicates, and collagen fiber. Jellification of tannins is another way for inhibition of dissolution of tannin in aqueous media [14]. Although the ability of tannins for removal of heavy metals is well-known facts, few researchers have studied the dye removal capacity with tannins. Recent researches have shown that tannin is one of the best adsorbent for the removal of dyes and heavy metals from aqueous solutions. Natural tannin-based adsorbent could be synthesized based on the jellification of Quebracho bark tannin. It has been shown that Quebracho tannin gel (QTG) adsorbent could be utilized for removal of cationic dye such as Methylene Blue (MB) from aqueous solution [15].

In 2012, Bagda conducted an investigation to remove two cationic dye (i.e. Basic Blue 9 and Basic Violet 3) by a low-cost biosorbent, namely Rosa Canina Galls [16]. In this work, the effect of parameters such as pH, adsorbent dosage, and initial dye concentration was examined. From the thermodynamic analysis, he also showed that the adsorption process was endothermic and the adsorption process follows the Freundlich model and the pseudo-second-order kinetic.

Bagda and co-workers synthesized a polymer called croyogels from the Rosa canina gall extract for removal of tetracycline from aqueous solution [17]. The croyogels had some remarkable characteristics such as lightweight, thin polymeric walls, interconnected large pores, and sponge like nature. From the equilibrium data, they concluded that Langmuir and Freundlich isotherms are the dominant models and kinetic of adsorption follows the pseudo-second-order kinetic model. Thermodynamic studies also showed that the adsorption process was exothermic and spontaneous. Furthermore, the adsorption rate was relatively high and equilibrium time was reached after 40–50 min [17].

In another study, Esra Bagda et al. employed the Quercus macranthera galls extract to prepare the croyogels for the removal of tetracycline from aqueous solution [18]. They showed that the adsorbent was lightweighted, spongy, and with a high adsorption capacity. From the thermodynamic analysis, they also concluded that the adsorption of tetracycline on the croyogels was exothermic and spontaneous. They also revealed that the Freundlich and Langmuir isotherms were compatible with the equilibrium data. Furthermore, the kinetics of tetracycline adsorption was moderately fast and would almost reach equilibrium in 150 min and the kinetic model was pseudo-second-order. Adsorption of Pb(II) on modified quebracho tannin resin (QTR) was investigated by Meral Yurtsever and Ayhan Sengil [19]. They found that QTR could be used as a proper adsorbent for the removal of Pb ions from aqueous solution and it has high adsorption capacity. Some researchers considered mesoporous silicates as a suitable insoluble supports for immobilization of water-soluble agents. Some studies have been conducted on the removal of dyes and heavy metal ions by mesoporous substances. Mesoporous materials have a large surface area, high mesoporous volume and narrow pore size distribution. Modification of the mesoporous substance surface with different types of functional groups has a significant effect on the adsorption efficiency of adsorbent and could be achieved by grafting or *in situ* synthesis routes. High specific surface area of mesoporous substance creates uniform and proper distribution of functional groups on its surface and pores. Liu et al. [20] synthesized silica nanoparticles modified by quaternary ammonium polyethylenimine as a new adsorbent for the removal of methyl orange from aqueous solution. Asouhidou et al. [21] synthesized hexagonal mesoporous silicate (HMS), aminopropyl modified HMS (HMS-NH_2) and b-cyclodextrin modified HMS (HMS-CD). These adsorbents were studied for the removal of Remazol Red 3BS. They concluded that the HMS-CD adsorbent had a higher adsorption capacity compared with the HMS-NH_2 and HMS. Mahmoodi et al. [22] synthesized silica nanoparticles (SN) and amine-functionalized silica nanoparticles (AFSN) and examined the abilities of these adsorbents for the removal of acid red 14 (AR14), acid black 1 (AB1), and acid blue 25 (AB25). They concluded that the dye removal capacity of SN for AR14, AB1, and AB25 was higher than that of AFSN. Qingdong et al. [23] synthesized ammonium-functionalized MCM-41 (NH_3^+-MCM-41) and investigated the adsorption of

Methyl orange (MO), Orange IV (OIV), Reactive brilliant red X-3B (X-3B), and Acid fuchsine (AF) onto the adsorbent. They revealed that the adsorption capacity of dyes follows the order of MO > OIV > AF > X-3B. Tannins could be immobilized on the surface of some materials to prevent their dissolution in aqueous media. Preparation of tannin-immobilized mesoporous silica (BT–SiO_2) was also investigated by Xin Huang and co-workers to remove chromium cations from aqueous media [24].

Applications of tannins are limited as an adsorbent due to low specific surface area. They show good adsorption capacity but consume long times to access equilibrium state. As indicated earlier, mesoporous silicate materials such as HMS have a high surface area and could be utilized as a proper support for the uniform distribution of tannin. Up to now, no instances have been reported in the literature for the utilization of HMS loaded by oak gall tannin for removal of DY86 from aqueous solution. Therefore, it is the aim of this study to extract the oak gall tannin and examine the adsorption capacity of DY86 on the oak gall tannin-immobilized hexagonal mesoporous silicate (OGT-HMS) adsorbent. Furthermore, adsorption isotherms, thermodynamics, and kinetics of the adsorption process would also be investigated to examine the adsorption mechanism.

2. Materials and methods

2.1. Materials

Tannin was extracted from oak gall powder using a mixture of water and methanol with a ratio of 1:1 as a solvent in this paper. The solvent was then evaporated at 60˚C and a pressure of 10 mm Hg [25]. It was found that the extraction yield was 82.08%. The tannin contents of the extract were found to be 26.14 and 15.27% using Lowenthal and Folin–Ciocalteu methods, respectively, based on gallic acid. In the Lowenthal method, tannin acts as a reductant and it is titrated by permanganate with a given normality. In order to determine the finish point, the indigo carmine reagent is used. A color change of the solution from blue to yellow is the sign of end of titration [26]. On the other hand, Folin–Ciocalteu method is one of the fastest and easiest techniques for the determination of phenolic compounds. The Folin–Ciocalteu reagent is mixture of phosphomolybdate and phosphotungstate. Therefore, if the sample contains phenolic compounds, it could reduce the tungstate or molybdate from +6 to +5 [27]. Folin–Denis reagent was utilized in Folin–Ciocalteu method.

The utilized reagents/materials in this paper were tetraethyl ortho silicate (TEOS, $SiC_8H_{20}O_4$), ethanol (C_2H_5OH), methanol (C_2H_3OH), hydrochloric acid (HCl), dodecylamine ($C_{12}H_{25}NH_2$), 3-Aminopropyltriethoxysilane, potassium permanganate ($KMnO_4$), and sodium carbonate (Na_2CO_3), H_2SO_4 and NaOH for the adjustment of pH, Na_2HPO_4, and NaH_2PO_4 for the preparation of buffer solution and deionized water. All the materials were purchased from Merck and Folin–Denis and indigo carmine reagents from Sigma–Aldrich. Furthermore, anionic dye (i.e. DY86 with $\lambda_{max} = 384$ nm) was obtained from Dystar, Germany. The chemical structure of DY86 is shown in Fig. 1.

2.2. Synthesize of HMS nanoparticles

HMS nanoparticle was synthesized using the procedure described by Tanev and Pinnavaia [28]. To prepare HMS, 3.50 g dodecyl amine as the surfactant, 1.40 ml HCl and 46.00 mL of deionized water were stirred in the vessel for 5 min. Then, it was added to a solution comprising 21.00 g of ethanol and 15.04 g TEOS, and stirred for 30 min. The mixture was then stirred for 6 h and left for 18–24 h at room temperature. Next, the prepared gel was filtrated, washed with deionized water, and dried at 100˚C for 6 h in a vacuum oven. The dried gel was then calcinated in a furnace at 600˚C for 6 h where the rate of furnace temperature was set at 100˚C.

2.3. Preparation of aminated HMS

The aminated HMS nanopowder was synthesized using HMS powder, hexane and 3-aminopropyltriethoxysilane (APTES) as follows:

About 1.00 g of HMS and 10 mL of APTES were stirred with 50 mL of normal hexane. It was carried out under the reflux for 6 h. Then, the prepared nanoparticles were filtered, washed with acetone and deionized water, and finally dried for 24 h under vacuum at 323 K [29].

2.4. Preparation of tannin-HMS adsorbent

Due to high nucleophilic tendency of the phenolic rings, electrophilic agents such as glutaraldehyde could form covalent bond with the existing rings,

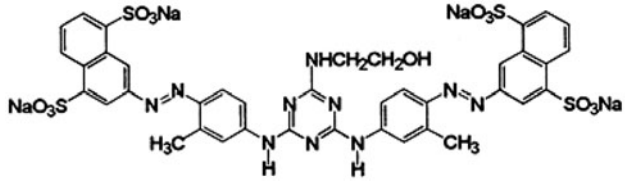

Fig. 1. Chemical structure of DY86.

where glutaraldehyde could also react with the amino group of aminated HMS. Therefore, immobilization of tannin on aminated HMS nanopowders occurs with glutaraldehyde as the cross-linking agent and hence the covalent bond forms [30].

After preparation of 0.3, 0.6, and 1% oak gall tannin solutions, 1.00 g of the prepared aminated HMS nanopowder was mixed with tannin solutions. The mixtures were then stirred for 2 h at room temperature. Next, 4 mL of glutaraldehyde (50%, w/w) was added to the mixtures. Then, the mixtures were stirred for 24 h at 298 K. Afterward, the mixtures were filtered, washed with deionized water and dried in a vacuum oven at 323 K where brown tannin-HMS nanopowder was obtained. Tannin grafting extent of HMS could be assessed based on the concentration difference of tannin solution before and after the loading where it was measured using ultraviolet-visible spectrophotometer (6310, JENWAY, UK). The result reveals that the loading of HMS by 1% oak gall tannin solution was 38.5%, which was the highest amount of loading. It must be noted that in order to ensure reproducibility of the results, the preparation of OGT-HMS nanopowder was repeated several times. Fig. 2 shows the trend of the tannin-HMS nanopowder synthesis.

2.5. Characterization

X-ray diffraction (XRD) analysis of samples were carried out in the range of $2\theta = 0^{\circ}$–80° using refractometer (XRD, Philips instruments, Australia). The operating conditions were 35 kV, 28.5 mA, and 25°C where copper anode was used as a radioactive source. In this paper, dye solutions were analyzed using UV–visible spectrophotometer prior and after the adsorption of DY86 on the adsorbent. The BET surface area was evaluated from the linear part of BET plot. Pore size and pore volume distributions were also estimated from the adsorption curve of N_2 adsorption-desorption isotherm by BJH (Barret–Joyner–Halenda) method (Quantachrome NovaWin2, USA). Transmission electron microscopy (TEM) images of the adsorbent were prepared (TEM, CM120, PHILIPS, Holland) operating at 150 kV. The presence of tannin as the functional group on the surface of HMS was exhibited by fourier transform infrared spectrometry (FTIR, 8400S, Shimadzu, Japan) in the wave numbers ranging from 400 to 4,000 cm^{-1} using KBr technique. In order to compute the amount of tannin on the HMS and thermal resistance of samples, thermogravimetric analysis (TGA) was carried out in the temperature ranging from 15 to 700°C, by heating rate of 10°C and in the presence of air flow (TGA-25, Shimatzu, Japan).

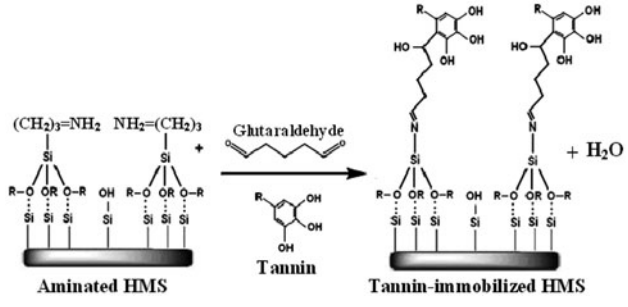

Fig. 2. Synthesis trend for OGT-HMS adsorbent.

2.6. Batch adsorption procedure

DY86 removal tests were carried out in a 250 mL erlenmeyer flask containing 50 mL of dye solutions for initial concentrations of 40, 60, 80, 100, 120, and 200 mg L^{-1}. Dye solutions were prepared in phosphate buffer of 0.1 M. Each flask was holding the optimal dosage of OGT-HMS nanopowder at the optimum pH. All tests were conducted in a shaker incubator at different initial dye concentrations. The effects of pH, adsorbent dosage, initial dye concentrations, contact time, and temperature on the dye removal were also investigated.

For each concentration and after 15, 30, 45, 60, 90, 120, and 180 min of contact time, samples were taken and centrifuged at 5,000 rpm for 30 min. In order to assess the amount of dye that has not been removed from the solution, ultraviolet-visible spectrophotometer was applied. The adsorption capacity of DY86 on adsorbent was obtained through the following relationship:

$$q_t = (C_i - C_t) \times V/M \quad (1)$$

where q_t (mg/g) is the adsorption capacity at time t, C_i, and C_t (mg/L) are dye solution concentrations at initial time and any time t, V, and M are volume of dye solution (L) and mass of adsorbent (g), respectively.

Batch equilibrium tests were also carried out in order to determine the adsorption of dye onto OGT-HMS at equilibrium. The adsorption capacity at equilibrium was evaluated using the following equation:

$$q_e = (C_i - C_e) \times V/M \quad (2)$$

where C_e mg L^{-1} is the dye concentration at equilibrium. The removal efficiency was also calculated as follows:

$$\text{Removal efficiency } (\%) = (C_i - C_t)/C_i \times 100 \quad (3)$$

where C_i and C_t are the initial and terminal concentrations of solutions, respectively.

3. Results and discussion

3.1. Characterization of tannin-HMS adsorbent

TEM image of OGT-HMS adsorbent is also shown in Fig. 3, where the light and dark spots are the indications of pores of HMS and immobilized tannin and have been designated by white and black arrows. The sizes of these pores are less than 5 nm and are verified by BET analysis.

The FTIR spectra of HMS and OGT-HMS were prepared in the range of 400–4,000 cm^{-1}. These graphs are utilized in order to compare them and obtain some insights into the immobilization of tannin on the HMS. For the HMS, Fig. 4 demonstrates the structure of Si-OH groups with the water molecules that have been adsorbed in the range of 3,000–3,700 cm^{-1} and with a broad band. The sharp peak at 1,087 cm^{-1} is the indication of Si–O-Si vibrations (asymmetric stretch) and the peaks at 465 and 802 cm^{-1} demonstrate the bending and symmetric stretch, respectively [31,32]. For the OGT-HMS as an adsorbent, the presence of broadband in the range of 3,000–3,700 cm^{-1} and peak at 3,443 cm^{-1}, exhibits the stretching vibration of –OH (i.e. phenolic and alcoholic groups) in the tannin as well as –OH groups in the hydrogen-bonded water molecules. The peak at 2,925 cm^{-1} is the indication of the methylene (–CH_2–) bridges and aromatic C–H stretching vibrations [33,34]. The sharp peak at 2,363 cm^{-1} could be caused due to the carboxyl group compound on the OGT-HMS [35]. Furthermore, the peaks in the vicinity of 1,450–1,650 cm^{-1} are the indication of aromatic rings [36]. The absorption band at 1,088 cm^{-1} demonstrates the stretching vibrations of C–O–C [37]. It must be noted that these bands do not indicate the spectrum of HMS; however, demonstrate the loading of tannin onto the HMS.

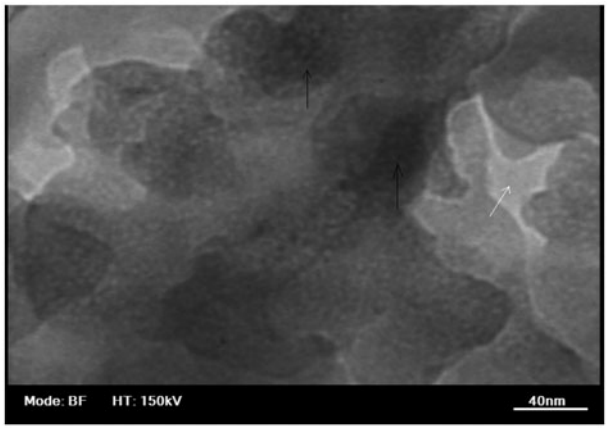

Fig. 3. TEM image of OGT-HMS adsorbent (white and black arrows show pores of HMS and immobilized tannin).

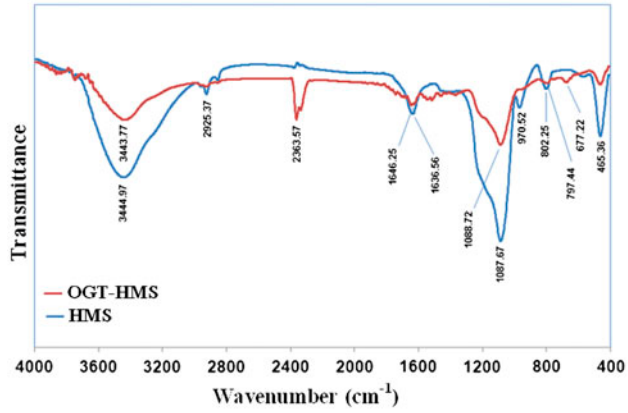

Fig. 4. FTIR spectrums of the HMS and OGT-HMS.

The reduction of peak intensities in the range of 3,000–3,700 cm^{-1} and at 1,087 cm^{-1} also signifies that HMS nanopowder forms. It was also found that HMS contains more OH groups in comparison with the tannin-immobilized HMS per unit area. It was also noted the immobilization of tannins on the surface of HMS causes a reduction in total number of OH per unit area. However, the stretching vibration at the wave number of 3,443.77 cm^{-1} and the peak intensity of OH would die down.

Fig. 5 demonstrates the X-ray diffraction (XRD) patterns of HMS and OGT-HMS. It shows that at the peak of $2\theta < 5^\circ$, the HMS has been formed [28,38]. Moreover, the broad band in the range of $2\theta = 20^\circ$–30° signifies that the base is amorphous and the presence of two peaks shows the formation of HMS nanoparticles [39,40]. From the XRD patterns of OGT-HMS and HMS, it was concluded that both spectra have a similar peaks at $2\theta < 5^\circ$ which demonstrates that the adsorbent had HMS nanoparticles in its structure.

In order to study the thermal resistance of the HMS and estimation of HMS loading by tannin, TGA was carried out. As Fig. 6 demonstrates, HMS lost 3–4% of its weight in the temperature range of 50–700°C. For OGT-HMS, 44% of weight loss occurred in the temperature range of 50–700°C due to the evaporation of existing water in tannin and destruction of tannin functional groups. These weight loss exhibits that tannin is immobilized onto HMS and synthesized adsorbent contains 56% HMS and 44% organic phase. To determine the specific surface area and pore size.

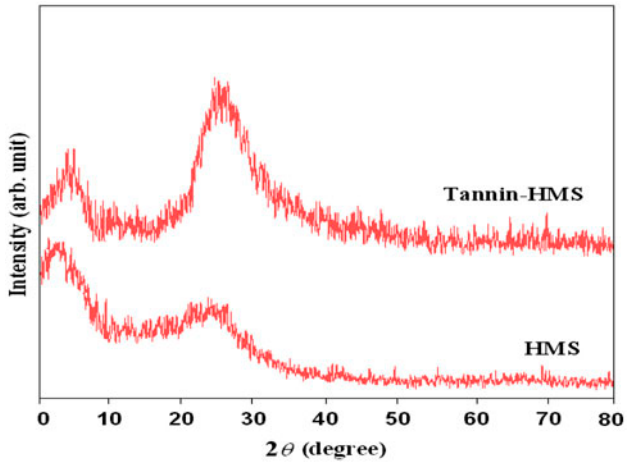

Fig. 5. XRD patterns of the HMS and OGT-HMS.

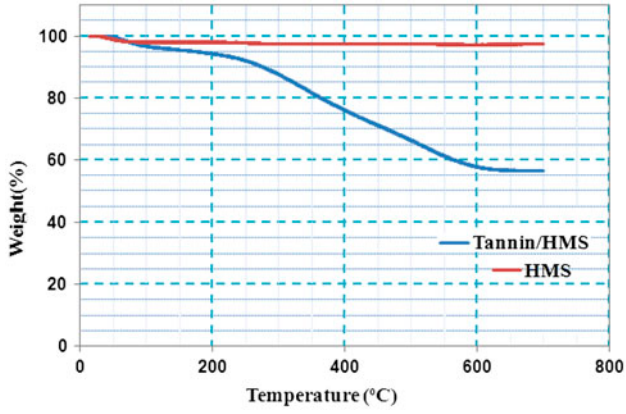

Fig. 6. TGA experiment at 50–700˚C.

Distribution of the synthesized adsorbent, the BET curve in the adsorption data and BJH analysis were used and the results are shown in Table 1.

The N_2 adsorption–desorption isotherms for HMS and OGT-HMS are shown in Fig. 7. As can be seen, for the HMS, sharp increase at P/P_o values between 0.2 and 0.40 occurred. This is because of capillary condensation inside of the mesopores of HMS that has similar size (narrow pore size distribution of HMS nanoparticles can be seen in the inset of Fig. 7). Thus, adsorption isotherm of IV-type can be expressed for HMS. The sharp increment of N_2 adsorption at $P/P_o > 0.93$ is a characteristic feature of HMS and it is related to the presence of macropores [21,41]. As shown in the Fig. 7, N_2 adsorption isotherm for OGT-HMS kept its form according to the IV type with a difference in N_2 adsorption step and due to the coverage of the mesopores by tannin. The pore size distribution of OGT-HMS was partly broad and the pore diameter (4.246 nm) was slightly larger than that of HMS (2.920 nm) (inset in Fig. 7), meaning pore size of HMS modified by oak gall tannin, which has been changed slightly and remains constant less than 5 nm. The uniform pore size distributions of HMS and OGT-HMS also demonstrate that there were no defects in the pore structure after loading of HMS by tannin. Moreover, the desorption part shows a hysteresis between $P/P_o = 0.91$ and 0.50, showing of the presence of ink-bottle type of pores [21]. The results in Table 1 also revealed that the surface area and pore volume of HMS after coating by tannin decreased 94.56 and 84.03%, respectively, signifying the proper coverage of HMS by tannin.

3.2. Effect of pH on the adsorption capacity

Optimization was carried out at pH in the range 2–10 with the initial dye concentration of 40 ppm, 0.025 g of adsorbent and the contact time of 90 min in this paper. From Fig. 8, it was concluded that the maximum dye removal was occurred at a pH 2. At low pH, the concentration of H^+ ions increases in the system and the tannin would also get positive with the absorption of H^+. Since the adsorbent surface is positively charged at lower pH values, the strong electrostatic attraction between the positive charges of the adsorbent and the negative charges of dye molecules leads to the maximum adsorption of dye. If the pH increases, the number of negative charges of the sites

Table 1
Characterization results of HMS and OGT-HMS

Samples	S_{BET}[a] (m^2/g)	Internal area[b] (m^2/g)	External[b] surface area (m^2/g)	D_p[c] (nm)	V_p[d] (cm^3/g)
HMS	885.400	688.679	196.751	2.920	1.190
OGT-HMS	51.080	3.098	47.985	4.246	0.190

[a]Specific surface area, calculate from multi point BET analysis.
[b]Internal area and external surface area calculated from *V*–*t* plot (de-Boer method).
[c]The pore diameter calculated from the adsorption part of the isotherm using the BJH method.
[d]Total pore volume.

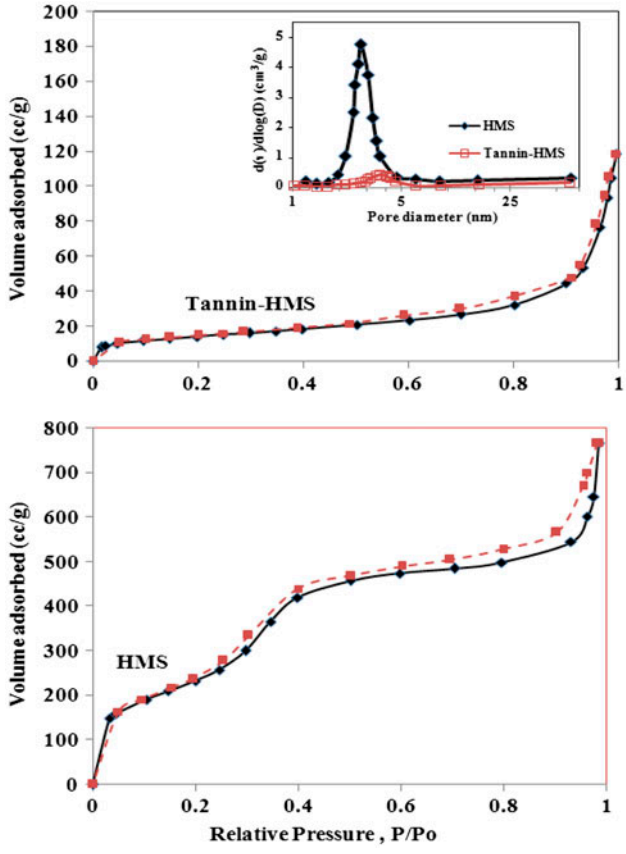

Fig. 7. N_2 adsorption–desorption isotherms and pore volume distribution (inserts) of HMS and OGT-HMS.

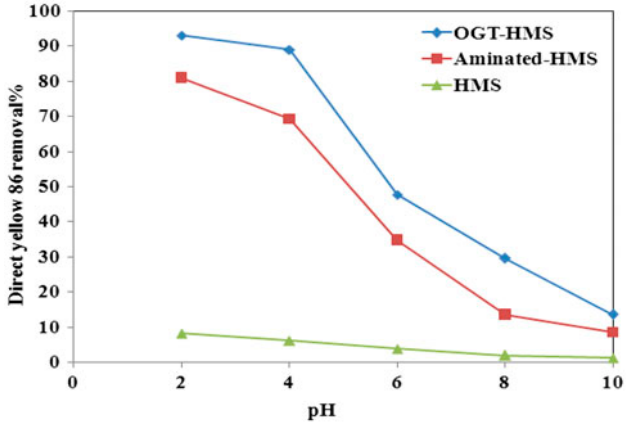

Fig. 8. Effect of pH on the percentage of dye removal by OGT-HMS (adsorbent dosage: 0.025 g in 50 mL dye solutions, initial DY86 concentration: 40 mg/L, contact time: 90 min, and T: 20˚C).

increase and positive charges decrease, so the electrostatic repulsion of negatively charged tannin and molecules of anionic dye leads to lower adsorption of dye [42]. The low adsorption of DY86 in alkaline environment was due to the competition between OH^- ions and anionic dye molecules to be adsorbed on the sites.

3.3. Adsorption mechanism of DY86 onto tannin-HMS

The adsorption mechanism of DY86 onto OGT-HMS is demonstrated in Fig. 9 and is as follows: ionic solubility of dye in aqueous solution and releases positive and negative ions; protons attack to the hydroxyl groups of tannin; ion exchange between the negatively charged DY86, and formation of OH_2^+ groups on tannin structure.

3.4. Effect of initial dye concentration

Fig. 10(a) demonstrates that the percentage of dye removal decreases with an increase the initial dye concentration from 40 to 200 ppm. The initial dye concentration provides the required driving force to overcome the mass transfer resistance between the liquid and solid phase. An enhancement in the initial dye concentration improves the interaction between DY86 and adsorbent and increases adsorption capacity (q_e) (Fig. 10(b)) [43]. Mesoporous silicate coated by oak gall tannin showed the maximum adsorption capacity and the highest dye removal percentage in comparison with aminated HMS and HMS.

3.5. Effect of adsorbent dosage

The findings of the present study revealed that with the enhancement of adsorbent up to the optimum value, the percentage of dye removal increases accordingly; however, it becomes steady beyond this point. This phenomenon could be manifested due to extra accumulation of adsorbent that leads to a reduction of the acceptor sites and inhibition of the adsorption [43]. This also could be attributed to the screening effect in the vicinity of the adsorbent. Mashithan and

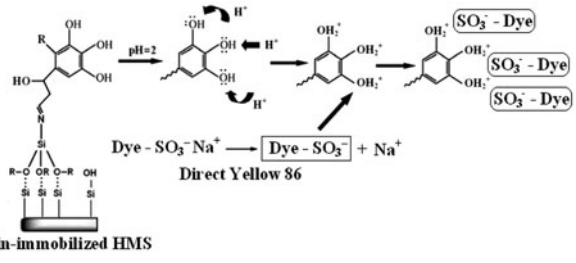

Fig. 9. The proposed mechanism for adsorption of DY86 onto OGT-HMS.

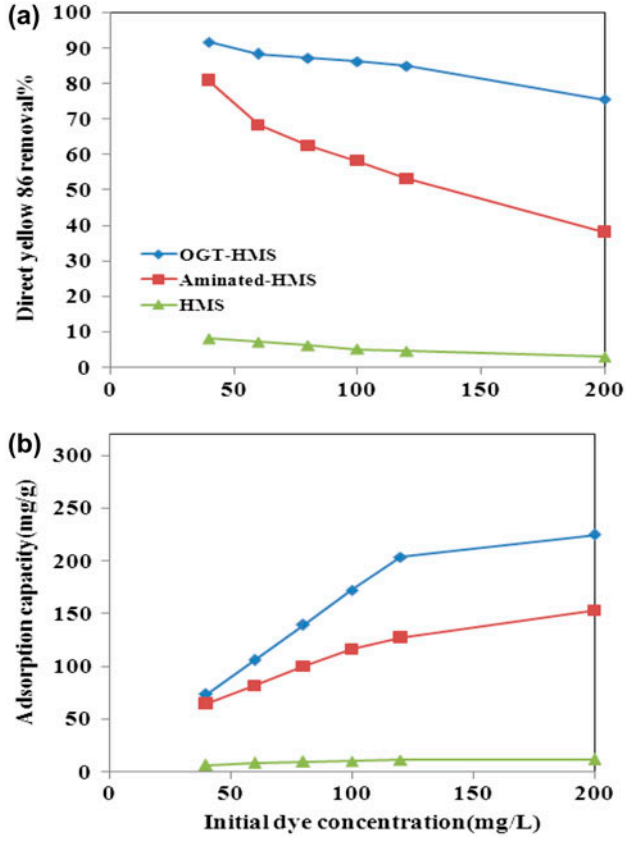

Fig. 10. Effect of initial dye concentration on the percentage of dye removal (a) and adsorption capacity (b). (initial dye concentration: 40 up to 200 ppm, adsorbent dosage: 0.025 g in 50 mL of dye solutions, contact time: 90 min, and *T*: 20˚C).

Yahya have also investigated the biosorption of copper ions. They reported that high concentration of the biosorbent could exhibit a screening effect in the outer layer of the cell and would hence protect the binding sites from the copper ions uptake. Therefore, the copper removal capacity would be decreased accordingly [44,45]. In this paper, the measurements were carried out in the presence of 0.01, 0.015, 0.02, 0.025, 0.05, 0.075, 0.1, and 0.15 g of OGT-HMS adsorbent with the initial dye concentration of 40 ppm, pH of 2.0, and temperature of 20˚C. Fig. 11 shows the effect of the adsorbent dosage on dye removal. It was found that the optimum amount of adsorbent was 0.025 g, which was also utilized for the rest of the work.

3.6. Effect of contact time

As Fig. 12 demonstrates, the adsorption process occurs instantly for all concentrations in the first 15 min. Following the first 15 min and up to 90 min, adsorption would be completed and beyond that the adsorption equilibrium would be achieved. The results showed that an enhancement of the contact time from 90 to 180 min had no significant effect on the dye adsorption. Thus, 90 min contact time was considered as the equilibrium time and was utilized for the rest of the work. With an increase in the contact time, the aggregation of dye molecules occurs on the surface of OGT-HMS. Therefore, deep penetration of dye into the sites having higher energies is impossible. The single, smooth, and continuous adsorption curves are the indication of the saturation condition and monolayer coverage of the adsorbent surface by DY86 [46].

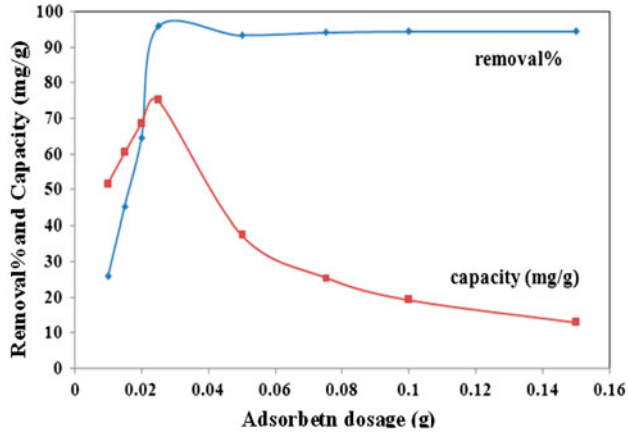

Fig. 11. Effect of adsorbent dosage on the percentage of dye removal and adsorption capacity (initial DY86 concentration: 40 ppm, pH 2, contact time: 90 min, and *T*: 20˚C).

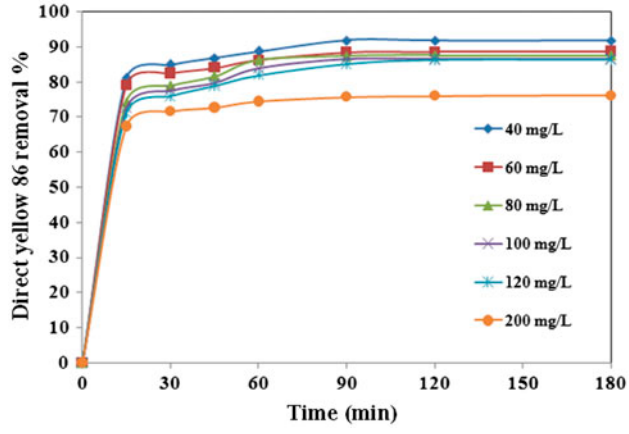

Fig. 12. Effect of contact time on the percentage of dye removal (initial dye concentration: 40 up to 200 ppm, adsorbent dosage: 0.025 g in 50 mL of dye solutions, pH 2, and *T*: 20˚C).

3.7. Effect of temperature on the dye removal

In order to examine the effects of temperature on the adsorption of DY86 onto the adsorbent, experiments were carried out at temperatures of 293, 303, 313, and 323 K. The initial dye concentrations were 40–200 mg/L with 0.025 g of the OGT-HMS adsorbent and for equilibrium time of 90 min. Fig. 13 shows that the percentage of dye removal decreases with the increase of concentrations while increasing with the enhancement of temperature up to 323 K. This phenomenon could be primarily caused due to the increase in surface activity, since adsorption of DY86 onto tannin-HMS adsorbent is an endothermic process.

3.8. Effect of temperature on the thermodynamic parameters

Thermodynamic parameters such as ΔG°, ΔH°, and ΔS° could be calculated from the following equations [42,43]:

$$K_c = C_{Ae}/C_e \quad (4)$$

$$\Delta G^{\circ} = -RT \ln k_c \quad (5)$$

$$\Delta G^{\circ} = \Delta H^{\circ} - T\Delta S^{\circ} \quad (6)$$

$$\log k_c = \Delta S^{\circ}/2.303R - \Delta H^{\circ}/2.303RT \quad (7)$$

In these equations, k_c, C_e, and C_{Ae} are the equilibrium constant, the equilibrium concentration in solution (mg/L), and amount of adsorbed dye on the adsorbent per liter of solution in the equilibrium state, respectively. In the above equations, ΔG°, ΔH°, and ΔS° are the changes in Gibbs free energy, enthalpy, and entropy with the units of kJ/mol and J/mol K, respectively. Furthermore, the values of ΔH° and ΔS° could be obtained from the slope and intercept of the plot of log k_c vs. $1/T$, shown in Fig. 14 and the ΔG° could be obtained from Eq. (6). It was concluded that sorption of DY86 onto OGT-HMS adsorbent was enhanced with increase in temperature from 293 K up to 323 K; therefore, the adsorption process was endothermic. The values of thermodynamic parameters (ΔG°, ΔH°, and ΔS°) at different temperatures and different initial concentrations are shown in Table 2. Negative values of ΔG° indicate that the adsorption process is feasible and spontaneous. As Table 2 demonstrates, with the increase of temperature, Gibbs free energy becomes more negative and this signifies the fact that the enhancement of temperature causes promotes the spontaneity of the adsorption process. However, an increase of the initial dye concentration would make lower the Gibbs free energy, which is an indication of the fall in the spontaneous adsorption process. The positive magnitude of the ΔH° shows that the adsorption is endothermic. Therefore, the magnitude of the heat of adsorption (ΔH°) could specify the type of adsorption.

Adsorption process is categorized in two major physical and chemical types. Since the involved forces in physical adsorption are weak, the heat of adsorption for the physical adsorption would be less than that of 21 kJ/mol. However, involved forces in chemical adsorption are stronger than that of physical adsorption and heat of chemical adsorption like heat of chemical reactions is about 21–42 kJ/mol [42,43].

According to the values obtained for the ΔH°, the adsorption of DY86 onto OGT-HMS is the physical

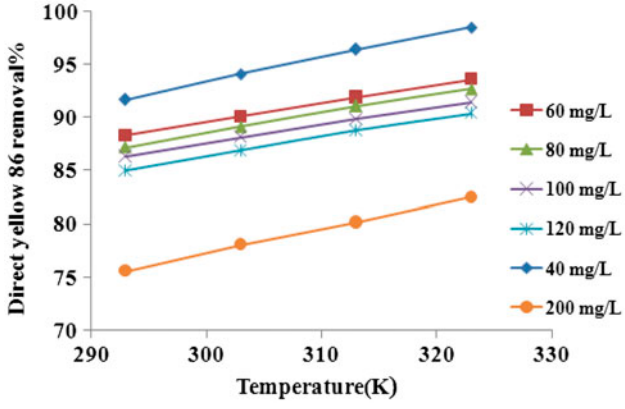

Fig. 13. Effect of temperature on the percentage of dye removal (initial dye concentration: 40 up to 200 ppm, adsorbent dosage = 0.025 g in 50 mL of dye solutions, pH 2, and contact time: 90 min).

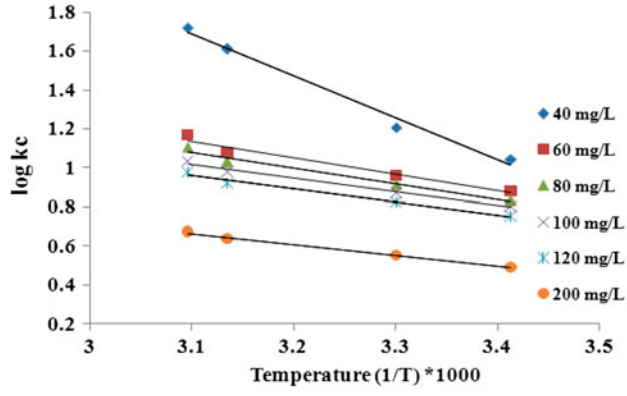

Fig. 14. Effect of temperatures in the range of 293–323 K on the thermodynamical parameters (initial dye concentration: 40–200 ppm, adsorbent dosage: 0.025 g in 50 mL of dye solutions, pH 2, contact time: 90 min).

Table 2
Thermodynamic parameters for the adsorption of DY86 onto the OGT-HMS

Initial DY86 concentration (mg/L)	ΔH° (kJ/mol)	ΔS° (J/mol K)	ΔG° (kJ/mol)			
			20℃	30℃	40℃	50℃
60	16.140	71.780	−4.930	−5.570	−6.330	−7.220
80	15.450	68.600	−4.680	−5.310	−6.060	−6.840
100	13.350	60.810	−4.500	−5.060	−5.680	−6.370
120	12.780	58.050	−4.230	−4.770	−5.390	−6.030
200	10.680	45.860	−2.760	−3.200	−3.650	−4.170

adsorption. From the magnitude of the ΔS°, it was utilized to express the randomness of DY86 adsorption process in the adsorbent-solution interface in this paper. A positive value of ΔS° indicates an increase in the irregularities in the interface of solution-adsorbent during the adsorption process, which implies an enhancement of the efficiency. Results of some other research demonstrated that adsorption of direct dyes onto different adsorbents has positive values for entropy and enthalpy changes [46,47].

3.9. Adsorption isotherm models

Capacity of adsorption isotherms is a major issue and plays an important role in determination of maximum adsorption capacity. Adsorption isotherms indicate the effectiveness of the adsorbent during adsorption process and provide possibility of economic assessment of commercial applications of adsorbent for removal of some specific solutes. Parameters of isotherms were calculated using nonlinear regression in the present paper.

3.9.1. The Langmuir isotherm

In the present work, the Langmuir isotherm was employed in order to determine the adsorption capacity. The Langmuir isotherm is based on several key assumptions such as monolayer adsorption and similarity of the energy for all of the active sites [13].

The non linear form of Langmuir isotherm is shown below:

$$q_e = q_m k_L C_e/(1 + k_L C_e) \quad (8)$$

where q_e is the equilibrium adsorption capacity of adsorbent (mg g^{-1}), C_e is the equilibrium concentration (mg/L). In Eq. (8), the term q_m signifies to the maximum adsorption capacity of the adsorbent (mg/g). Furthermore, the Langmuir constant (k_L) is a coefficient that correlates the adsorbent to the adsorbate. High amounts of k_L values indicate the binding affinity for the dye molecules.

3.9.2. The Freundlich isotherm

This model is based on empirical data on the nature and is available for heterogeneous surfaces (surfaces having active sites with different adsorption energies) [13]. Freundlich model exhibits that energy of adsorption decreases exponentially on the active sites of an adsorbent. The Freundlich isotherm is expressed as follows:

$$q_e = k_f C_e^{1/n} \quad (9)$$

Constant of Freundlich isotherm, k_f is used for relative evaluation of the adsorption capacity (L g^{-1}). Constant n shows adsorption intensity and $1/n$ is the heterogeneity factor of the surface. High values of k_f express readily of adsorption of dye molecules from aqueous solutions and high values of n indicate suitable and desirable adsorption. The value of n below to unity shows that adsorption is chemical process. If the value of n is equal to unity, the adsorption is linear. The values of n in the range of 2–10 suggest a favorable and physical adsorption.

3.9.3. The Redlich–Peterson isotherm

The Redlich–Peterson isotherm is a hybrid isotherm describing both Langmuir and Freundlich isotherms [48]. This is a three parameteric model as an empirical equation. This model is compatible with the Freundlich isotherm at high concentrations and shows consistency with the Langmuir model at low concentrations. The Redlich–Peterson model is presented as follows:

$$q_e = k_R C_e/(1 + \alpha_R\ C_e^{\beta}) \quad (10)$$

where k_R (L g^{-1}), α_R (L mg^{-1}) and β are Redlich–Peterson constants and equation exponent, respectively. The Freundlich isotherm will be a predominant isotherm when β tends to zero and the Langmuir model will be a preferable isotherm if the value of β is close to unity.

3.9.4. Dubinin–Radushkevich isotherm

The isotherm equation is as follows [49]:

$$q_e = q_m e^{-\beta\varepsilon 2} \quad (11)$$

where q_m is monolayer adsorption capacity of Dubinin–Radushkevich (mg g^{-1}), β is a constant related to the adsorption energy, and e is the Polanyi potential that is related to the equilibrium concentration:

$$\varepsilon = RT\ln(1 + 1/C_e) \quad (12)$$

where R and T are the gas constant (8.314 J/mol K) and absolute temperature, respectively. β and ε are mean free energy and adsorption per each adsorbed molecule when this molecule is transferred to a solid surface, respectively. Relationship between ε and β is defined as below:

$$\varepsilon = 1/[(2\beta)^{0.5}] \quad (13)$$

3.9.5. The Temkin isotherm

Temkin isotherm was used to study the multilayer adsorption. The isotherm has been presented in the below form [50,51]:

$$q_e = B\ln(AC_e) \quad (14)$$

In this paper, experimental data of DY86 adsorption onto adsorbent were fit on the isotherm models using MATLAB software. In Fig. 15, graphical representations of these models are shown. Parameters of different isotherms were calculated from the nonlinear regression principle and are presented in Table 3. It was found that there exists a good compatibility between the experimental data and the results of models and could hierarchically be ranked based on the R^2 values as follows:

Langmuir (0.994) > Freundlich (0.983) > Redlich–Peterson (0.960) > Temkin (0.892) > Dubinin–Radushkevich (0.833). As Table 3 illustrates, Langmuir isotherm has the highest correlation coefficient, signifying that the monolayer adsorption has occurred and acceptor groups of adsorbate are uniformly and homogeneously distributed on the surface of the adsorbent. For Freundlich isotherm n is equal to 2, which is the indication of proper adsorption. Since the correlation coefficient of Freundlich isotherm was high (i.e. 0.983), the Redlich–Peterson isotherm model, which is the combination of Langmuir and Freundlich isotherms model was adopted in this paper. It was also found that the correlation coefficient for the Redlich–Peterson isotherm was 0.96 which was lower than that of Langmuir isotherm; therefore, Langmuir isotherm was still predominant. To extend the investigation to other isotherm models, the Dubinin–Radushkevich isotherm was also examined. The correlation coefficient for Dubinin–Radushkevich isotherm was found to be 0.833, which was still lower than that of Langmuir isotherm. Therefore, from the above isotherm models considered in this paper, it could be concluded that the Langmuir isotherm was the best. To study the multilayer adsorption, Temkin isotherm was also examined. The correlation coefficient of Temkin model was found to be 0.892, which signifies it is monolayer adsorption; therefore, the Langmuir model is predominant.

The dimensionless parameter R_L in the Langmuir isotherm is one of the effective parameters in the model that is expressed by Eq. (15) [52]:

$$R_L = 1/(1 + bC_0) \quad (15)$$

where C_0 and b are the initial dye concentration and Langmuir constant, respectively. The types of

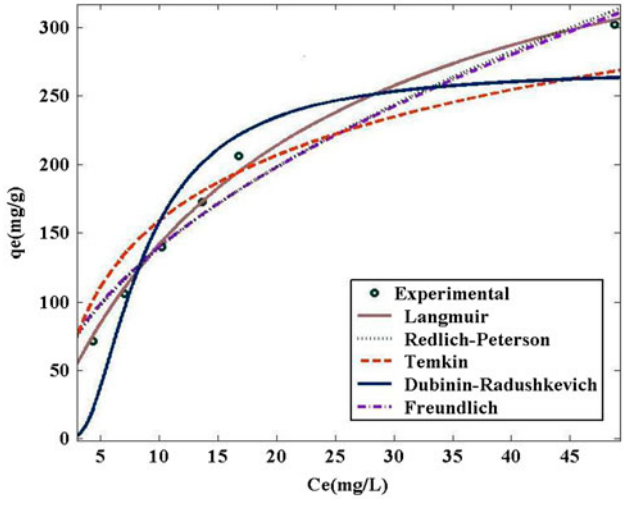

Fig. 15. The non linear adsorption isotherms for DY86 with OGT-HMS at 293 K.

Table 3
The values of parameters for each isotherm model

Isotherm model	Parameters from nonlinear regression	R^2	Equations
Langmuir $q_e = q_m K_L C_e/(1 + K_L C_e)$	$q_m = 435.500$ $K_l = 0.048$	0.994	$q_e = 20.900C_e/\ (1 + 0.048C_e)$
Freundlich $q_e = K_f C_e^{1/n}$	$K_f = 44.090$ $n = 2$	0.983	$q_e = 44.090C_e^{0.5}$
Redlich–Peterson $q_e = k_R C_e/\ (1 + a_R C_e^{\beta})$	$K_R = 2.222$ $\alpha_R = 0.052$ $\beta = 0.489$	0.960	$q_e = 2.222C_e/\ (1 + 0.052C_e^{0.489})$
Temkin $q_e = B \ln\ (AC_e)$	$B = 88.960$ $A = 0.680$	0.892	$q_e = 88.960\ \ln\ 0.680C_e$
Dubinin–Radushkevich $q_e = q_m e^{-\beta e2}$	$q_m = 268.800$ $\beta = 9.930\ mol^2/kJ^2$ $E = 1/[(2\beta)^{0.5}] = 0.224\ kJ/mol$	0.833	$q_e = 268.1e^{-9.930e2}$

adsorption, which is classified according to the values of R_L, are listed in Table 4.

The values of R_L for the Langmuir isotherm are shown in Table 5, which demonstrates that the adsorption of DY86 onto the OGT-HMS was a favorable.

For comparative purposes, the maximum value of monolayer adsorption capacity of some direct dyes onto different adsorbents was also tabulated in Table 6. The results in Table 6 reveal that the OGT-HMS adsorbent has a large capacity of adsorption. This was due to high BET specific surface area of HMS, presence of high amounts of phenolic groups in oak gall tannin structure and uniform distribution of tannin on HMS. These reasons are caused the reduction of the BET specific surface area of HMS from 885.40 to 51.08 m^2/g, after the loading through tannin.

3.10. Adsorption kinetics

Studying on the kinetic of adsorption is an important factor in the investigation of the adsorption process. To predict the adsorption mechanism and determination of the controlling steps of adsorption such as mass transfer and chemical reaction, kinetic models must be utilized. In order to determine the kinetic model governing the adsorption process, the intraparticle diffusion model, pseudo-first-order and pseudo-second-order models must be employed.

Table 4
Effect of R_L values on adsorption quality

Adsorption quality	R_L
Unfavorable adsorption	$R_L > 1$
Favorable adsorption	$0 < R_L < 1$
Irreversible adsorption	$R_L = 0$
Linear adsorption	$R_L = 1$

3.10.1. Intraparticle diffusion model

This kinetic model is based on the model that was presented by Weber and Morris [57], where the diffusion model is expressed using the following equation:

$$q_t = k_p t^{0.5} + C \tag{16}$$

where C and k_p are the intercept and intraparticle diffusion rate constant ($mg\ g^{-1}\ min^{-0.5}$), respectively. In Eq. (16), k_p is the slope of the line which is obtained from plotting q_t values (mg/g) vs. $t^{0.5}$ and the intercept value indicates the boundary layer effects. With an increase in the intercept values, contribution of adsorption on the controlling step of the rate will increase. Table 7 demonstrates the values of k_p obtained from the findings of the present study. It reveals that the diffusion rate increases with the enhancement of initial dye concentration, which is caused due to the high driving force values and the increase of C_0. If graphs from linear regression of q_t values against $t^{0.5}$ pass through the origin, intraparticle diffusion is the only rate-controlling step. However, as demonstrated in Fig. 16, the linear graphs do not pass through the origin. Therefore, intraparticle diffusion is not the only rate-controlling step and other kinetic mechanisms may control the adsorption rate, which is proven with other studies of adsorption [1,3].

Boundary layer effects increase with the increase of initial dye concentration. Therefore, as the equations for diffusion illustrates, when the intraparticle

Table 5
Values of R_L for the adsorption of DY86 on OGT-HMS at 293 K and different initial concentrations

Langmuir isotherm	40 mg/L	60 mg/L	80 mg/L	100 mg/L	120 mg/L	200 mg/L	40 mg/L
R_L from nonlinear regression	0.342	0.257	0.206	0.172	0.148	0.094	0.342

Table 6
Comparison of maximum monolayer adsorption of direct dyes onto different adsorbents

Dyes	Adsorbents	q_m (mg/g)	References
Direct yellow 12 (DY-12)	Cadmium oxide nanowires loaded on activated carbon (CdO-NW-AC)	357.14	[1]
Direct yellow 86 (DY86)	Carbon nanotubes (CNTs)	56.20	[3]
Direct red 224 (DR224)	Carbon nanotubes (CNTs)	61.30	[3]
Direct Yellow 86 (DY86)	*Tannin loaded on HMS (OGT-HMS)*	*435.50*	*This study*
Direct blue 106 (DB106)	Loofa egyptiaca (LE)	73.53	[53]
Direct yellow 12 (DY-12)	Orange peel activated carbon	75.76	[54]
Direct yellow 12 (DY-12)	Silver nanoparticles loaded activated carbon (SNP-AC),	454.54	[55]
Direct yellow 161 (DY-161)	Bamboo activated carbons	4.62	[56]

Table 7
Comparison of the constants of pseudo-first-order, pseudo-second-order, intraparticle kinetic models, experimental and calculated values of adsorption capacity (q_e) at different initial concentrations of DY86

Initial DY86 concentration (mg/L)	Pseudo-first-order			Pseudo-second-order				Intraparticle diffusion		
	k_{ad} (1/min)	$q_{e,cal.}$ (mg/g)	R^2	k_h (g/mg.min)	$q_{e,cal.}$ (mg/g)	$q_{e,exp.}$ (mg/g)	R^2	K_p (mg/g.min$^{0.5}$)	C (mg/g)	R^2
40	0.026	32.900	0.996	0.004	76.920	73.384	0.999	1.516	59.120	0.994
60	0.029	68.380	0.976	0.003	111.111	106.116	0.997	2.023	87.230	0.992
80	0.031	82.140	0.990	0.001	66.666	139.568	0.997	3.872	104.700	0.956
100	0.033	105.520	0.990	0.001	200.000	172.720	0.999	5.065	126.000	0.979
120	0.029	146.430	0.990	0.001	250.000	205.704	0.998	6.296	146.700	0.996
200	0.027	192.020	0.988	0.001	333.333	303.120	0.998	6.930	249.700	0.942

diffusion is the only rate-controlling step, the rate constant (k_p) has a direct relationship with the square root of the initial dye concentration $C_0^{0.5}$ [13]. The variation of k_p with $C_0^{0.5}$ is plotted in Fig. 17. It was concluded that the graph is not a straight line; hence, the intraparticle diffusion is not the only rate-controlling step.

3.10.2. The pseudo-first-order kinetic model

Pseudo-first-order model was suggested by Lagergren where this model is expressed using the following equation [58]:

$$dq/dt = k_1(q_e - q) \quad (17)$$

After the integration of the above equation and rearranging, the following linear form was obtained:

$$\ln(q_e - q) = \ln(q_e) - k_1 t \quad (18)$$

In the Lagergren pseudo-first-order model, q_e (mg g^{-1}) and rate constant k_{ad} (min^{-1}) were calculated at different concentrations from the plot of $\ln(q_e - q_t)$ vs. t as shown in Fig. 18 and the findings are listed in Table 7.

3.10.3. The pseudo-second-order kinetic model

Pseudo-second-order kinetic model of Ho has also been investigated which is given by the following equation [58]:

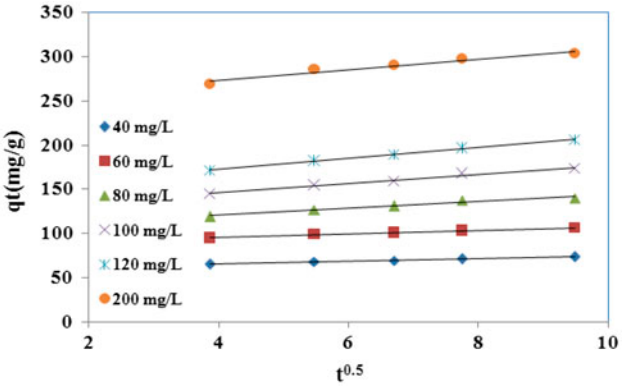

Fig. 16. Intraparticle diffusion model for adsorption of DY86 onto the OGT-HMS at 293 K.

$$dq/dt = k_h(q_e - q)^2 \quad (19)$$

Integrating of the above equation and rearranging, the following linear form was obtained:

$$t/q = 1//k_h q_e^2 + t/q_e \quad (20)$$

From the plot of the values of t/q_t vs. t and as are shown in Fig. 19, straight lines are obtained where the values of q_e and k_h could be estimated from the slope and intercept values. As demonstrated previously (Table 7), it could be concluded that the pseudo-second-order model has the highest correlation coefficient.

Comparative study between the pseudo-first and pseudo-second-order models reveals that although both modes have a high correlation coefficient; nonetheless, the pseudo-second-order model has a higher

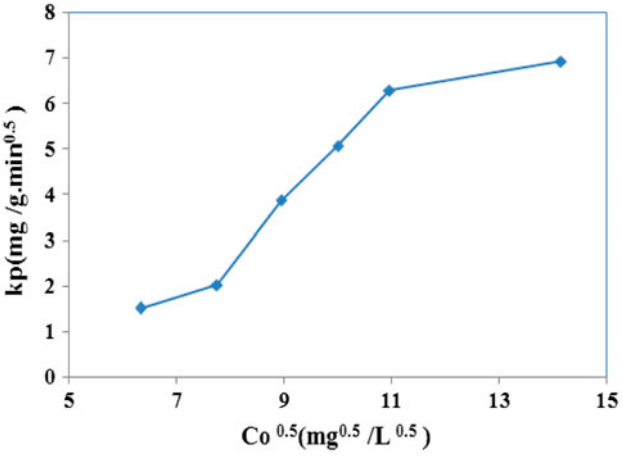

Fig. 17. Variation of K_p with $C_0^{0.5.}$

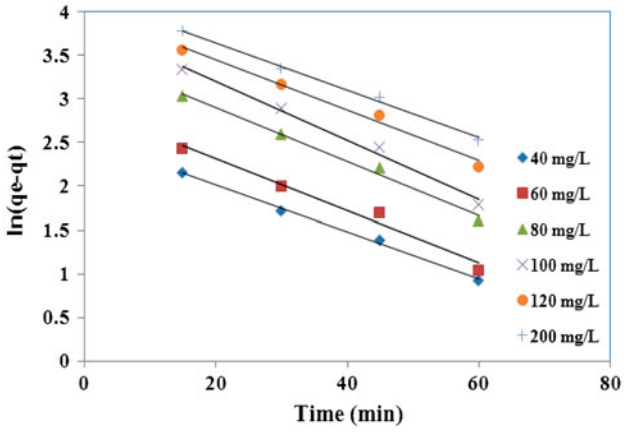

Fig. 18. Pseudo-first-order kinetic model for adsorption of DY86 onto the OGT-HMS at 293 K.

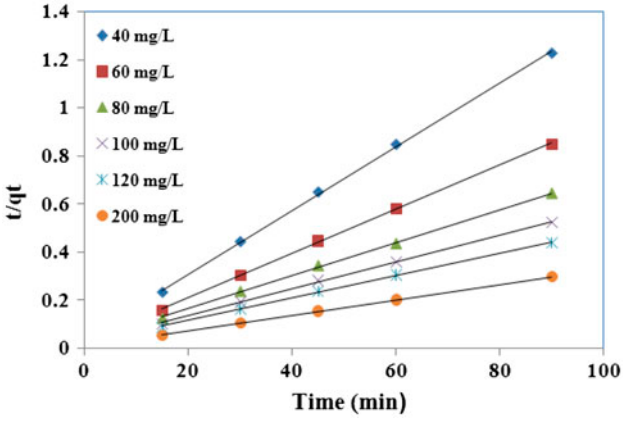

Fig. 19. Pseudo-second-order kinetic model for adsorption of DY86 onto the OGT-HMS at 293 K.

value. However, it must be noted that values of q_e calculated from the pseudo-second-order model ($q_{e,cal.}$) are more analogous to the experimental data ($q_{e,exp.}$); hence, the pseudo-second-order kinetic model is the predominant model in the adsorption process. Similar reports have been published by previous researchers for removal of direct yellow 12 by cadmium oxide nanowires loaded on activated carbon (CdO-NW-AC) [1], DY86 removal on carbon nanotubes [3] and adsorption of direct yellow 12 onto silver nanoparticles loaded activated carbon (SNP-AC) [55].

4. Conclusion

In this paper, tannin was extracted from oak gall and was immobilized onto HMS, and was then employed as a new composite adsorbent (OGT-HMS)

for the removal of DY86. Evaluation of phenolic contents of extracted tannin was performed by Folin–Ciocalteu and Lowenthal methods. The findings of this study revealed that the OGT-HMS had a high adsorption capacity and rapid adsorption rate for the dye removal. This was achieved by proper loading of HMS by tannin and was confirmed by the FTIR spectroscopy and TGA analysis. It was also concluded from the specific surface area obtained from the BET equation, volume and average pore size from the BJH method that the tannin is well distributed on the surface and in the pores of the adsorbent. Therefore, the synthesized OGT-HMS could be proclaimed as one of the best absorbent for dye removal. It has been shown that the interaction between DY86 and adsorbent has also been improved and the capacity of dye removal has also been enhanced accordingly. It was also concluded that the temperature had a direct effect on the dye removal and as the temperature at different concentrations increases, the percentage of dye removal would be enhanced accordingly. It was also shown that the adsorption process is endothermic and spontaneous.

In this paper, the equilibrium data were examined using Langmuir, Freundlich, Redlich–Peterson, Temkin, Dubinin–Radushkevich isotherms and parameters of each isotherm and the correlation coefficients were calculated using nonlinear regression. Furthermore, the isotherm models could hierarchically be ranked based on the R^2 values as follows:

Langmuir (0.994) > Freundlich (0.983) > Redlich–Peterson (0.960) > Temkin (0.892) > Dubinin–Radushkevich (0.833). The intraparticle diffusion model was also investigated. It was concluded that both boundary layer and intraparticle diffusion affects the adsorption process. It was also found that there exists a good compatibility between the pseudo-second-order kinetic model of the present paper and the experimental data.

Acknowledgements

The authors gratefully acknowledge the cooperation and helpful suggestions of Dr Habib Allah Tayebi from Department of Textile Engineering, Islamic Azad University, Qaemshahr Branch, Qaemshahr, Iran.

References

[1] M. Ghaedi, B. Sadeghian, S.N. Kokhdan, A.A. Pebdani, R. Sahraei, A. Daneshfar, A. Mihandoost, Study of removal of Direct Yellow 12 by cadmium oxide nanowires loaded on activated carbon, Mater. Sci. Eng., C 33 (2013) 2258–2265.

[2] G. Crini, Non-conventional low-cost adsorbents for dye removal: A review, Bioresour. Technol. 97 (2006) 1061–1085.

[3] C.Y. Kuo, C.H. Wu, J.Y. Wu, Adsorption of direct dyes from aqueous solutions by carbon nanotubes: Determination of equilibrium, kinetics and thermodynamics parameters, J. Colloid Interface Sci. 327 (2008) 308–315.

[4] Z. Aksu, I.A. Isoglu, Use of agricultural waste sugar beet pulp for the removal of Gemazol turquoise blue-G reactive dye from aqueous solution, J. Hazard. Mater. 137 (2006) 418–430.

[5] M.H. Baek, C.O. Ijagbemi, S.J. O, D.S. Kim, Removal of Malachite Green from aqueous solution using degreased coffee bean, J. Hazard. Mater. 176 (2010) 820–828.

[6] B.H. Hameed, A.A. Ahmad, Batch adsorption of methylene blue from aqueous solution by garlic peel, an agricultural waste biomass, J. Hazard. Mater. 164 (2009) 870–875.

[7] B.H. Hameed, M.I. El-Khaiary, Removal of basic dye from aqueous medium using a novel agricultural waste material: Pumpkin seed hull, J. Hazard. Mater. 155 (2008) 601–609.

[8] V. Dulman, S.M. Cucu-Man, Sorption of some textile dyes by beech wood sawdust, J. Hazard. Mater. 162 (2009) 1457–1464.

[9] P. Pengthamkeerati, T. Satapanajaru, O. Singchan, Sorption of reactive dye from aqueous solution on biomass fly ash, J. Hazard. Mater. 153 (2008) 1149–1156.

[10] T. Akar, I. Tosun, Z. Kaynak, E. Ozkara, O. Yeni, E.N. Sahin, S.T. Akar, An attractive agro-industrial by-product in environmental cleanup: Dye biosorption potential of untreated olive pomace, J. Hazard. Mater. 166 (2009) 1217–1225.

[11] A. Khaled, A. Nemr, A. El-Sikaily, O. Abdelwahab, Removal of Direct N Blue-106 from artificial textile dye effluent using activated carbon from orange peel: Adsorption isotherm and kinetic studies, J. Hazard. Mater. 165 (2009) 100–110.

[12] N. Gupta, A.K. Kushwaha, M.C. Chattopadhyaya, Application of potato (*Solanum tuberosum*) plant wastes for the removal of methylene blue and malachite green dye from solution, Arabian J. Chem. (2011) in press.

[13] Özlem Tunç, H. Tanacı, Z. Aksu, Potential use of cotton plant wastes for the removal of Remazol Black B reactive dye, J. Hazard. Mater. 163 (2009) 187–198.

[14] M. Özacar, İ. Ayhan Şengil, H. Türkmenler, Equilibrium and kinetic data and adsorption mechanism for adsorption of lead onto valonia tannin resin, Chem. Eng. J. 143 (2008) 32–42.

[15] J. Sánchez-Martín, M. González-Velasco, J. Beltrán-Heredia, J. Gragera-Carvajal, J. Salguero-Fernández, Novel tannin-based adsorbent in removing cationic dye (Methylene Blue) from aqueous solution. Kinetics and equilibrium studies, J. Hazard. Mater. 174 (2010) 9–16.

[16] E. Bağda, The feasibility of using Rosa canina galls as an effective new biosorbent for removal of methylene blue and crystal violet, Desalin. Water Treat. 43 (2012) 63–75.

[17] E. Bağda, M. Erşan, E. Bağda, Investigation of adsorptive removal of tetracycline with sponge like, *Rosa canina* gall extract modified, polyacrylamide cryogels, J. Environ. Chem. Eng. 1 (2013) 1079–1084.

[18] M. Erşan, E. Bağda, E. Bağda, Investigation of kinetic and thermodynamic characteristics of removal of tetracycline with sponge like, tannin based cryogels, Colloids Surf., B 104 (2013) 75– 82.
[19] M. Yurtsever, İ. Ayhan Şengil, Biosorption of Pb(II) ions by modified quebracho tannin resin, J. Hazard. Mater. 163 (2009) 58–64.
[20] J. Liu, S. Ma, L. Zang, Preparation and characterization of ammonium-functionalized silica nanoparticle as a new adsorbent to remove methyl orange from aqueous solution, Appl. Surf. Sci. 265 (2013) 393–398.
[21] D.D. Asouhidou, K.S. Triantafyllidis, N.K. Lazaridis, K.A. Matis, Adsorption of Remazol Red 3BS from aqueous solutions using APTES- and cyclodextrin-modified HMS-type mesoporous silicas, Colloids Surf., A 346 (2009) 83–90.
[22] N.M. Mahmoodi, S. Khorramfar, F. Najafi, Amine-functionalized silica nanoparticle: Preparation, characterization and anionic dye removal ability, Desalination 279 (2011) 61–68.
[23] Q. Qingdong, J. Ma, K. Liu, Adsorption of anionic dyes on ammonium-functionalized MCM-41, J. Hazard. Mater. 162 (2009) 133–139.
[24] X. Huang, X. Liao, B. Shi, Tannin-immobilized mesoporous silica bead (BT–SiO_2) as an effective adsorbent of Cr(III) in aqueous solutions, J. Hazard. Mater. 173 (2010) 33–39.
[25] M. Labieniec, T. Gabryelak, Interactions of tannic acid and its derivatives (ellagic and gallic acid) with calf thymus DNA and bovine serum albumin using spectroscopic method, J. Photochem. Photobiol., B 82 (2006) 72–78.
[26] E.V. Trease, Pharmacognosy, W.B. Saunders publications, London, 1966, pp. 224–232.
[27] K. Slinkard, V.L. Singleton, Total phenol analysis: Automation and comparison with manual methods, Am. J. Enol. Vitic. 28 (1977) 49–55.
[28] P.T. Tanev, T.J. Pinnavaia, A neutral templating route to mesoporous molecular sieves, Science 267 (1995) 865–867.
[29] K.Y. Ho, G. McKay, K.L. Yeung, Selective adsorbents from ordered mesoporous silica, Langmuir 19 (2003) 3019–3024.
[30] X. Huang, Y. Wang, X. Liao, B. Shi, Adsorptive recovery of Au^{3+} from aqueous solutions using bayberry tannin-immobilized mesoporous silica, J. Hazard. Mater. 183 (2010) 793–798.
[31] C.Z.S. Luo, W.Q. Pang, Y.W. Fan, X.H. Chen, F.Z. Cui, Dilute solution routes to various controllable morphologies of MCM-41 silica with a basic medium, Chem. Mater. 13 (2001) 258–263.
[32] M. Sarkar, P.K. Acharya, B. Bhattacharya, Modeling the adsorption kinetic of some priority organic pollutants in water from diffusion and activation energy parameters, J. Colloid Interface Sci. 266 (2003) 28–32.
[33] L. Falcão, M. Araújo, M. Araujo, Tannins characterization in historic leathers by complementary analytical techniques ATR-FTIR, UV–vis and chemical tests, J. Cultural Heritage 14 (2013) 499–508.
[34] L.I. Grishechko, G. Amaral-Labat, A. Szczurek, V. Fierro, B.N. Kuznetsov, A. Pizzi, A. Celzard, New tannin–lignin aerogels, Ind. Crops Prod. 41 (2013) 347–355.
[35] M.C.E. Bulut, A. Ornek, M. Ozacar, Synthesis and characterization of valonea tannin resin and its interaction with palladium (II), rhodium (III) chloro complexes, Chem. Eng. J. 221 (2013) 146–158.
[36] M. Gurung, B.B. Adhikari, H. Kawakita, K. Ohto, K. Inoue, S. Alam, Recovery of Au(III) by using low cost adsorbent prepared from persimmon tannin extract, Chem. Eng. J. 174 (2011) 556–563.
[37] M. Yurtsever, Ayhan ŞENGL, Adsorption and desorption behavior of silver ions onto valonia tannin resin, Trans. Nonferrous Met. Soc. China 22 (2012) 2846–2854.
[38] P.T. Tanev, M. Chibwe, T.J. Pinnavaia, Titanium containing mesoporous molecular-sieve for catalytic-oxidation of aromatic-compounds, Nature 368 (1994) 321–323.
[39] W. Gac, A. Derylo-Marczewska, S. Pasieczna-Patkowska, N. Popivnyak, G. Zukocinski, The influence of the preparation methods and pretreatment conditions on the properties of Ag-MCM-41 catalysts, J. Mol. Catal. A: Chem. 268 (2007) 15–23.
[40] H. Zhao, J. Zhou, H. Luo, C. Zeng, D. Li, Y. Liu, Synthesis, characterization of Ag/MCM-41 and the catalytic performance for liquid-phase oxidation of cyclohexane, Catal. Lett. 108 (2006) 49–54.
[41] T.R. Pauly, T.J. Pinnavaia, Pore size modification of mesoporous HMS molecular sieve silicas with wormhole framework structures, Chem. Mater. 13 (2001) 987–993.
[42] M.M. Maria Rahman, N. Akter, M.R. Karim, N. Ahmad, M.M. Rahman, I.A. Siddiquey, N.M. Bahadur, M.A. Hasnat, Optimization, kinetic and thermodynamic studies for removal of Brilliant Red (X-3B) using Tannin gel, J. Environ. Chem. Eng. 2 (2014) 76–83.
[43] P.S. Senthil Kumar, S. Ramalingam, C. Senthamarai, M. Niranjanaa, P. Vijayalakshmi, S. Sivanesan, Adsorption of dye from aqueous solution by cashew nut shell: Studies on equilibrium isotherm, kinetics and thermodynamics of interactions, Desalination 261 (2010) 52–60.
[44] M.D. Mashitah, Z. Zulfadhfy, S. Bhatla, Ability of *Pycnoporus Sanguineus* to remove copper ions from aqueous solution, Artif. Cells, Blood Substitues, Immobilization Biotechnol. 27 (1999) 429–433.
[45] Y. Yahaya, M.M. Mat Don, S. Bhatia, Biosorption of copper (II) onto immobilized cells of *Pycnoporus sanguineus* from aqueous solution: Equilibrium and kinetic studies, J. Hazard. Mater. 161 (2009) 189–195.
[46] Q.Q. Zhong, Q.Y. Yue, Q. Li, X. Xu, B.Y. Gao, Preparation, characterization of modified wheat residue and its utilization for the anionic dye removal, Desalination 267 (2011) 193–200.
[47] N.A. Kamal, Removal of direct blue-106 dye from aqueous solution using new activated carbons developed from pomegranate peel: Adsorption equilibrium and kinetics, J. Hazard. Mater. 165 (2009) 52–62.
[48] O. Redlich, D.L. Peterson, A useful adsorption isotherms, J. Phys. Chem. 63 (1959) 1024–1024.
[49] M.M. Dubinin, L.V. Radushkevich, Equation of the characteristic curve of activated charcoal, Chem. Zentralbl. 1 (1947) 875–889.
[50] B.H. Hameed, Spent tea leaves: A new non-conventional and low-cost adsorbent for removal of basic dye from aqueous solutions, J. Hazard. Mater. 161 (2009) 753–759.

[51] M.J. Temkin, V. Pyzhev, Recent modifications to Langmuir isotherms, Acta Phys. chim. URSS. 12 (1940) 217–225.
[52] B.H. Hameed, R.R. Krishni, S.A. Sata, A novel agricultural waste adsorbent for the removal of cationic dye from aqueous solutions, J. Hazard. Mater. 162 (2009) 305–311.
[53] E.S.Z El Ashtoukhy, Loofa egyptiaca as a novel adsorbent for removal of direct blue dye from aqueous solution, J. Environ. Manage. 90 (2009) 2755–2761.
[54] A. Khaled, A.E. El Nemr, A.E. El-Sikaily, O. Abdelwahab, Treatment of artificial textile dye effluent containing Direct Yellow 12 by orange peel carbon, Desalination 238 (2009) 210–232.
[55] M. Ghaedi, B. Sadeghian, A. Pebdani, R. Sahraei, A. Daneshfar, C. Duran, Kinetics, thermodynamics and equilibrium evaluation of direct yellow 12 removal by adsorption onto silver nanoparticles loaded activated carbon, Chem. Eng. J. 187 (2012) 133–141.
[56] L.G. Wang, G.B. Yan, Adsorptive removal of direct yellow 161dye from aqueous solution using bamboo charcoals activated with different chemicals, Desalination 274 (2011) 81–90.
[57] W.J. Webr, J.C. Morris, Kinetics of adsorption on carbon from solution, J. Sanit. Eng. Div. Am. Soc. Civ. Eng. 89 (1963) 31–60.
[58] W. Li, Y. Tang, Y. Zeng, Z. Tong, D. Liang, W. Cui, Adsorption behavior of Cr(VI) ions on tannin-immobilized activated clay, Chem. Eng. J. 193–194 (2012) 88–95.